

Diphoton rate of the standard-model-Like Higgs boson in the extra $U(1)$ extended MSSM

Kingman Cheung^{1,2}, Chih-Ting Lu¹, and Tzu-Chiang Yuan³

¹*Department of Physics, National Tsing Hua University, Hsinchu 300, Taiwan*

²*Division of Quantum Phases & Devices, School of Physics,*

Konkuk University, Seoul 143-701, Republic of Korea

³*Institute of Physics, Academia Sinica, Nankang, Taipei 11529, Taiwan*

(Dated: February 26, 2024)

Abstract

Motivated by the excess in the diphoton production rate of the Higgs boson at the Large Hadron Collider (LHC), we investigate the possibility that one of the CP-even Higgs bosons of the extra $U(1)$ extended minimal supersymmetric standard model can give a consistent result. We scan the parameter space for a standard-model-like Higgs boson such that the mass is in the range of 124 – 127 GeV and the production rate $\sigma \cdot B$ of the WW^* , ZZ^* modes is consistent with the standard model (SM) values while that of $\gamma\gamma$ is enhanced relative to the SM value. We find that the SM-like Higgs boson is mostly the lightest CP-even Higgs boson and it has a strong mixing with the second lightest one, which is largely singletlike. The implications on $Z\gamma$ production rate and properties of the other Higgs bosons are also studied.

I. INTRODUCTION

A boson of mass 125 GeV, almost consistent with the standard model (SM) Higgs boson, was recently discovered at the LHC experiments [1, 2]. The production rates of $pp \rightarrow h \rightarrow WW^*, ZZ^*$ are consistent with the SM values while that of $pp \rightarrow h \rightarrow \gamma\gamma$ is somewhat higher than the SM expectation. On the other hand, fermionic modes $b\bar{b}$ and $\tau\tau$ seem to be suppressed in the present data set, however, the uncertainties are still too large to say anything concrete. Nevertheless, the diphoton rate has seemed to stay above the SM prediction since 2011. If it is confirmed after collecting more data at the end of 2012, this would become a strong constraint on supersymmetry models and on other extended Higgs models.

In the minimal supersymmetric standard model (MSSM), the mass of the lightest CP-even Higgs boson can be raised to 125 GeV by a large radiative correction with a relatively large soft parameter A_t [3, 4]. However, the more difficult requirement is to achieve an enhanced diphoton production rate $gg \rightarrow h \rightarrow \gamma\gamma$ relative to the SM prediction. One possibility is to have a light scalar tau (or stau), as light as 100 GeV, which is made possible by choosing the third generation slepton masses $m_{L_3}, m_{E_3} \sim 200 - 450$ GeV, the parameter $\mu \sim 200 - 1000$ GeV, and large $\tan\beta \sim 60$ [4]. Such a light stau will soon be confirmed or ruled out at the LHC. Another possibility is to identify the heavier CP-even Higgs boson as the observed 125 GeV boson ¹ and the enhancement of the diphoton rate is then made possible by a reduction in $b\bar{b}$ width [6]. In this case, all the other Higgs bosons are around or below 125 GeV, which will soon be uncovered at the LHC. Yet, one can also fine-tune the mixing angle (α) between the two CP-even Higgs bosons such that the observed one is mostly H_u , the Higgs doublet that couples to the right-handed up-type quarks. In this case, one can achieve enhancement to the diphoton rate and suppression to the $\tau\tau$ mode [7]. Among all these possible scenarios certain levels of fine-tuning are necessary to achieve a 125 Higgs boson and an enhanced diphoton rate.

It is quite well known that the next-to-minimal supersymmetric standard model (NMSSM) gives additional tree-level contributions to the Higgs boson mass arising from the terms $\lambda SH_u H_d$ and $\kappa S^3/3$ in the superpotential and the corresponding soft terms. The 125 GeV CP-even Higgs boson can be obtained as either the lightest or the second lightest one, with-

¹ A similar consideration was also analyzed for the two-Higgs-doublet models in Ref.[5].

out giving stress on the stop sector [8–10]. The diphoton production rate can be enhanced through the singlet-doublet mixing. The second lightest CP-even Higgs boson is the SM-like one while the lightest CP-even is more singletlike. The mixing between these two states substantially reduces the $b\bar{b}$ width of the SM-like Higgs boson, which then causes an increase of the branching ratio into $\gamma\gamma$ [8, 9].

In this work, we consider the $U(1)'$ -extended minimal supersymmetric standard model (UMSSM), which involves an extra $U(1)$ symmetry and a Higgs singlet superfield S . It is well known that by adding the singlet Higgs field one can easily raise the Higgs boson mass. The scalar component of the Higgs singlet superfield develops a vacuum expectation value (VEV), which breaks the $U(1)'$ symmetry and gives a mass to the $U(1)'$ gauge boson, denoted by Z' . At the same time, the VEV together with the Yukawa coupling can form an effective μ_{eff} parameter from the term $\lambda\langle S\rangle H_u H_d = \mu_{\text{eff}} H_u H_d$ in the superpotential, thus solving the μ problem of MSSM. Also, because of the presence of the $U(1)'$ symmetry, terms like S , S^2 , or S^3 are disallowed in the superpotential.

The existence of extra neutral gauge bosons had been predicted in many extensions of the SM [11]. String-inspired models and grand-unified theory (GUT) models usually contain a number of extra $U(1)$ symmetries, beyond the hypercharge $U(1)_Y$ of the SM. The exceptional group E_6 is one of the famous examples of this type. Phenomenologically, the most interesting option is the breaking of these $U(1)$'s at around TeV scales, giving rise to an extra neutral gauge boson observable at the Tevatron and the LHC. Previously, in the works of Refs.[12, 13], a scenario of $U(1)'$ symmetry breaking at around TeV scale by the VEV of a Higgs singlet superfield in the context of weak-scale supersymmetry was considered. The Z' boson obtains a mass from the breaking of this $U(1)'$ symmetry that is proportional to the VEVs. Such a Z' can decay into the SUSY particles such as neutralinos, charginos, and sleptons, in addition to the SM particles. Thus, the current mass limits are reduced by a substantial amount and so is the sensitivity reach at the LHC [12, 13]. We have also considered the SM-like boson and its decay branching ratios into WW^* , ZZ^* , and $\tilde{\chi}_1^0\tilde{\chi}_1^0$ with the Higgs boson mass in the ranges of 120 – 130 and 130 – 141 GeV [14]. In the first mass range 120 – 130 GeV, we selected the parameter space such that the SM-like Higgs boson behaves like the SM Higgs boson while in the second mass range 130 – 141 GeV, we selected the parameter space point to make sure that the Higgs boson is hiding from the existing data.

The goal in this work is to refine the previous analyses [14] to scan for the parameter space such that

1. the SM-like Higgs boson falls in the mass range $124 - 127$ GeV;
2. the production rates for $gg \rightarrow h \rightarrow WW^*, ZZ^*$ are consistent with the SM within certainties;
3. the production rate for $gg \rightarrow h \rightarrow \gamma\gamma$ is enhanced relative to the SM prediction, namely,

$$R_{\gamma\gamma} \equiv \frac{\sigma(gg \rightarrow h) \times B(h \rightarrow \gamma\gamma)}{\sigma(gg \rightarrow h_{\text{SM}}) \times B(h_{\text{SM}} \rightarrow \gamma\gamma)} > 1 ;$$

4. other existing constraints such as Z invisible width and chargino mass bound are fulfilled.

In the chosen parameter space, we calculate the $Z\gamma$ production rate and study the properties of the other Higgs bosons.

We organize the paper as follows. In the next section, we briefly describe the model (UMSSM) and summarize the formulas for the one loop decays of the CP-even Higgs bosons. In Sec. III, we search for the parameter space in the model that satisfies the above requirements, and present the numerical results. We discuss and conclude in Sec. IV. Detailed expressions for the loop functions in the decay formulas are relegated to the Appendix. Some recent studies on extended MSSM can be found in Ref. [15] and on extended electroweak models in Ref. [16].

II. UMSSM

For illustrative purposes we use the popular grand unified models based on the exceptional group E_6 , which is anomaly free. The two most studied $U(1)$ subgroups in the symmetry breaking chain of E_6 are

$$E_6 \rightarrow SO(10) \times U(1)_\psi, \quad SO(10) \rightarrow SU(5) \times U(1)_\chi$$

In E_6 each family of the left-handed fermions is embedded into a fundamental **27**-plet, which decomposes under $E_6 \rightarrow SO(10) \rightarrow SU(5)$ as

$$\mathbf{27} \rightarrow \mathbf{16} + \mathbf{10} + \mathbf{1} \rightarrow (\mathbf{10} + \mathbf{5}^* + \mathbf{1}) + (\mathbf{5} + \mathbf{5}^*) + \mathbf{1}$$

The SM fermions of each family together with an extra state identified as the conjugate of a right-handed neutrino are embedded into the **10**, **5***, and **1** of the **16**. All the other states are exotic states required for the **27**-plet of E_6 unification. In general, the two $U(1)_\psi$ and $U(1)_\chi$ are allowed to mix as

$$Q'(\theta_{E_6}) = \cos \theta_{E_6} Q'_\chi + \sin \theta_{E_6} Q'_\psi , \quad (1)$$

where $0 \leq \theta_{E_6} < \pi$ is the mixing angle. The commonly studied Z'_η model assumes the mixing angle $\theta_{E_6} = \pi - \tan^{-1} \sqrt{5/3} \sim 0.71\pi$ such that

$$Q'_\eta = \sqrt{\frac{3}{8}} Q'_\chi - \sqrt{\frac{5}{8}} Q'_\psi . \quad (2)$$

Here we follow the common practice by assuming that all the exotic particles, other than the particle contents of the MSSM, are very heavy and well beyond the reaches of all current and planned colliders. For an excellent review of Z' models, see Ref. [11].

The effective superpotential W_{eff} involving the matter and Higgs superfields in UMSSM can be written as

$$W_{\text{eff}} = \epsilon_{ab} [y_{ij}^u Q_j^a H_u^b U_i^c - y_{ij}^d Q_j^a H_d^b D_i^c - y_{ij}^l L_j^a H_d^b E_i^c + h_s S H_u^a H_d^b] , \quad (3)$$

where $\epsilon_{12} = -\epsilon_{21} = 1$, i, j are family indices, and y^u and y^d represent the Yukawa matrices for the up-type and down-type quarks respectively. Here Q, L, U^c, D^c, E^c, H_u , and H_d denote the MSSM superfields for the quark doublet, lepton doublet, up-type quark singlet, down-type quark singlet, lepton singlet, up-type Higgs doublet, and down-type Higgs doublet respectively, and S is the singlet superfield. The $U(1)'$ charges of the fields H_u, H_d , and S are chosen such that the relation $Q'_{H_u} + Q'_{H_d} + Q'_S = 0$ holds. Thus $S H_u H_d$ is the only term in the superpotential allowed by the $U(1)'$ symmetry beyond the MSSM. Once the singlet scalar field S develops a VEV, it generates an effective μ parameter: $\mu_{\text{eff}} = h_s \langle S \rangle$.

The singlet superfield will give rise to a singlet scalar boson and a singlino. The real part of the scalar boson will mix with the real part of H_u^0 and H_d^0 to form three physical CP-even Higgs bosons. The imaginary part of the singlet scalar will be eaten and become the longitudinal part of the Z' boson according to the Higgs mechanism in the process of spontaneous symmetry breaking of $U(1)'$. The singlino, together with the Z' -ino, will mix with the neutral gauginos and neutral Higgsinos to form six physical neutralinos. Studies of various singlet extensions of the MSSM can be found in Refs. [17–19].

The Higgs doublet and singlet fields are

$$H_d = \begin{pmatrix} H_d^0 \\ H_d^- \end{pmatrix} , \quad H_u = \begin{pmatrix} H_u^+ \\ H_u^0 \end{pmatrix} \quad \text{and} \quad S . \quad (4)$$

The scalar interactions are obtained by calculating the F - and D -terms of the superpotential, and by including the soft-SUSY-breaking terms. They are given in Refs. [12, 14].

Now we can expand the Higgs fields after taking on VEVs as

$$\begin{aligned} H_d^0 &= \frac{1}{\sqrt{2}} (v_d + \phi_d + i\chi_d) , \\ H_u^0 &= \frac{1}{\sqrt{2}} (v_u + \phi_u + i\chi_u) , \\ S &= \frac{1}{\sqrt{2}} (v_s + \phi_s + i\chi_s) . \end{aligned}$$

It is well known that the lightest CP-even Higgs boson mass receives a substantial radiative mass correction in the MSSM. The same is true here for the UMSSM. Tree-level and radiative corrections to the mass matrix $\mathcal{M}^{\text{tree}}$ have been given in Ref. [18]. We have included radiative corrections in our calculation. The interaction eigenstates ϕ_u, ϕ_d, ϕ_s can be rotated into mass eigenstates via an orthogonal matrix O

$$\begin{pmatrix} h_1 \\ h_2 \\ h_3 \end{pmatrix} = O \begin{pmatrix} \phi_d \\ \phi_u \\ \phi_s \end{pmatrix} , \quad (5)$$

such that $O\mathcal{M}^{\text{tree+loop}}O^T = \text{diag}(m_{h_1}^2, m_{h_2}^2, m_{h_3}^2)$ in ascending order. There are also one CP-odd Higgs boson and a pair of charged Higgs bosons, as in the MSSM. Note that the Higgs boson masses receive extra contributions from the D -term of the $U(1)'$ symmetry (proportional to g_2) and from the F -term for the mixing of the doublets with the singlet Higgs field (proportional to h_s).

A. Formulas for one loop decays of the CP-even Higgs bosons

We will present the relevant formulas for the one loop processes of $h_j \rightarrow \gamma\gamma, Z\gamma$ and gg . The gg width is relevant for the gluon-fusion production cross section. The couplings of the neutral CP-even Higgs bosons with the SM gauge bosons and fermions, charged Higgs bosons, sfermions, charginos and neutralinos have been given in Refs. [12, 14].

The $\gamma\gamma$ partial decay width of the CP-even Higgs boson (h_j , $j = 1, 2, 3$) receives contributions from all charged particles running in the loop. It is given by

$$\Gamma(h_j \rightarrow \gamma\gamma) = \frac{\alpha^2 m_{h_j}^3}{256\pi^3 v^2} \left| F_\tau + 3 \left(\frac{2}{3} \right)^2 F_t + 3 \left(-\frac{1}{3} \right)^2 F_b + F_W + F_{h^\pm} + F_{\tilde{\tau}} + 3 \left(\frac{2}{3} \right)^2 F_{\tilde{t}} + 3 \left(-\frac{1}{3} \right)^2 F_{\tilde{b}} + F_{\tilde{\chi}^\pm} \right|^2, \quad (6)$$

where the factor 3 in front of F_t , F_b , $F_{\tilde{t}}$, and $F_{\tilde{b}}$ accounts for the color factor, and $v^2 = v_u^2 + v_d^2$. The expressions for the loop functions F are given in the Appendix. For the decay $h_j \rightarrow gg$ where only colored particles are running in the loop, we have

$$\Gamma(h_j \rightarrow gg) = \frac{\alpha_s^2 m_{h_j}^3}{128\pi^3 v^2} \left| F_t + F_b + F_{\tilde{t}} + F_{\tilde{b}} \right|^2. \quad (7)$$

For the decay $h_j \rightarrow Z\gamma$, we have

$$\Gamma(h_j \rightarrow Z\gamma) = \frac{m_{h_j}^3}{32\pi} \left(1 - \frac{m_Z^2}{m_{h_j}^2} \right)^3 \frac{\alpha^2 g^2}{16\pi^2 m_W^2} \times \left| G_\tau + G_t + G_b + G_W + G_{h^\pm} + G_{\tilde{\tau}} + G_{\tilde{t}} + G_{\tilde{b}} + G_{\tilde{\chi}^\pm} \right|^2. \quad (8)$$

The expressions for the loop functions G are given in the Appendix.

III. SCANNING OF PARAMETER SPACE

The UMSSM has the following parameters: $M_{\tilde{Z}'}$, A_s , the VEV $\langle S \rangle = v_s/\sqrt{2}$, and the Yukawa coupling h_s , other than those of the MSSM: gaugino masses $M_{1,2,3}$, squark masses $M_{\tilde{q}}$, slepton masses $M_{\tilde{\ell}}$, soft parameters $A_{t,b,\tau}$, and $\tan\beta$. The soft parameter M_S can be expressed in terms of VEVs and couplings through the tadpole conditions. The effective μ parameter is given as $\mu_{\text{eff}} = h_s \langle S \rangle$. The other model parameters are fixed by the quantum numbers Q'_ϕ of various supermultiplets ϕ .

The mass of the Z' boson is determined by $m_{Z'} \approx g_2(Q_{H_u}'^2 v_u^2 + Q_{H_d}'^2 v_d^2 + Q_S'^2 v_s^2)^{1/2}$ if the $Z - Z'$ mixing is ignored. The most stringent limit on the Z' boson comes from the dilepton resonance search by ATLAS [2]. Nevertheless, we can avoid these Z' mass limits by assuming that the leptonic decay mode is suppressed. The mixing between the SM Z boson and the Z' can be suppressed by carefully choosing the $\tan\beta \approx (Q_{H_d}'/Q_{H_u}')^{1/2}$ [18]. In this work we do not impose these constraints in our parameter scan. However we note that we can always

carefully choose the set of quantum numbers Q' such that both the Z' mass and mixing constraints can be evaded.²

We first fix most of the MSSM parameters (unless stated otherwise):

$$\begin{aligned} M_1 &= M_2/2 = 0.2 \text{ TeV}, \quad M_3 = 2 \text{ TeV}; \\ M_{\tilde{Q}} &= 0.7 \text{ TeV}, \quad M_{\tilde{U}} = 0.7 \text{ TeV}, \quad M_{\tilde{D}} = 1 \text{ TeV}, \quad M_{\tilde{L}} = M_{\tilde{E}} = 1 \text{ TeV}; \\ A_b &= A_t = A_\tau = 1 \text{ TeV}. \end{aligned} \tag{9}$$

We also fix the UMSSM parameter:

$$A_s = 0.5 \text{ TeV}, \tag{10}$$

while we scan the rest of the parameters in the following ranges

$$0.2 < h_s < 0.6, \quad 1.1 < \tan \beta < 40, \tag{11}$$

and

$$0.2 \text{ TeV} < v_s < 2 \text{ TeV}, \quad 0.2 \text{ TeV} < M_{\tilde{Z}'} < 2 \text{ TeV}. \tag{12}$$

Note that the $U(1)'$ gaugino mass, $M_{\tilde{Z}'}$, is a soft-SUSY-breaking parameter, unlike the Z' boson mass which is fixed by the $U(1)'$ coupling constant and quantum numbers, and the three VEVs.

A. Constraints

Charginos mass.—The chargino sector of the UMSSM is the same as that of MSSM with the following chargino mass matrix

$$M_{\tilde{\chi}^\pm} = \begin{pmatrix} M_2 & \sqrt{2}m_W \sin \beta \\ \sqrt{2}m_W \cos \beta & \mu_{\text{eff}} \end{pmatrix}. \tag{13}$$

² Such a Z' boson is still subjected to the dijet resonance searches. The CMS Collaboration has published a search for dijet resonances [20], one of which is the Z' model with the SM couplings. The production cross section curve of the Z' barely touches the upper-limit curve and thus receives no constraint. The Z' boson in our case has a smaller coupling down by $g_2/g_1 \approx 0.62$, and so the production cross section is down by $(0.62)^2 = 0.38$. Similarly, it is true for the dijet resonance search in the mass range 260 – 1400 GeV by the CDF Collaboration [21], which ruled out a part of this Z' mass range when the Z' has the SM couplings. Again, in our case when the production cross section is down by 0.38, the constraint is moot. For an even lower mass range of dijet resonance search the relevant data came from UA2. However, for the Z' model with a coupling $g_2/g_1 = 0.62$ it has been shown to be safe with the UA2 data in [22].

Thus, the two charginos masses depend on M_2 , $\mu_{\text{eff}} = h_s v_s / \sqrt{2}$, and $\tan \beta$. The current bound for the lighter chargino mass is $m_{\tilde{\chi}_1^\pm} > 94$ GeV as long as its mass difference with the lightest supersymmetric particle (LSP) is larger than 3 GeV [23]. We impose this chargino mass bound in our scans in the parameter space defined by (11) and (12).

Invisible width of the Z boson.– The lightest neutralino $\tilde{\chi}_1^0$ is the LSP of the model, and thus would be stable and invisible. When the Z boson decays into a pair of LSPs, it would give rise to an invisible width of the Z boson, which had been tightly constrained by experiments. The current bound of the Z invisible width is $\Gamma_{\text{inv}}(Z) < 3$ MeV at about 95% C.L. [23]. The coupling of the Z boson to the lightest neutralino is given by

$$\mathcal{L}_{Z\tilde{\chi}_1^0\tilde{\chi}_1^0} = \frac{g_1}{4} (|N_{13}|^2 - |N_{14}|^2) Z_\mu \bar{\tilde{\chi}}_1^0 \gamma^\mu \gamma_5 \tilde{\chi}_1^0, \quad (14)$$

where N is the orthogonal matrix that diagonalized the neutralino mass matrix. The contribution to the Z boson invisible width is

$$\Gamma(Z \rightarrow \tilde{\chi}_1^0 \tilde{\chi}_1^0) = \frac{g_1^2}{96\pi} (|N_{13}|^2 - |N_{14}|^2)^2 m_Z \left(1 - \frac{4m_{\tilde{\chi}_1^0}^2}{m_Z^2}\right)^{3/2}. \quad (15)$$

Note that the Z boson would not couple to the singlino component, and we have assumed negligible mixing between Z and Z' bosons; therefore the Z boson would not couple to the Z' -ino component either. Here we impose the experimental constraint on the invisible Z width. The constraint of fulfilling the relic density by the LSP will be ignored in this work.

Mass of the Higgs boson and production rate of various decay modes.– The boson masses reported by CMS and ATLAS are 125.3 ± 0.6 [1] and 126.0 ± 0.6 GeV [2], respectively. The current data indicated that the observed boson is similar to the SM Higgs boson. For our purpose we define the SM-like Higgs boson $h_{\text{SM-like}}$ in our scenario when the square of its singlet component is smaller than $1/3$, i.e., $O_{k3}^2 < \frac{1}{3}$, where $h_k = O_{k1}\phi_d + O_{k2}\phi_u + O_{k3}\phi_s$. For all the allowed points we have $k = 1$ for the SM-like Higgs boson. We choose the allowable mass range for the SM-like Higgs boson in our analysis as

$$124 \text{ GeV} < m_{h_{\text{SM-like}}} < 127 \text{ GeV}. \quad (16)$$

The production rate of various channels of the Higgs boson relative to the SM prediction is defined as

$$R_{ab} \equiv \frac{\sigma(pp \rightarrow h + X) \times B(h \rightarrow ab)}{\sigma(pp \rightarrow h_{\text{SM}} + X) \times B(h_{\text{SM}} \rightarrow ab)} \quad (17)$$

where $ab = \gamma\gamma, W^+W^-, ZZ, b\bar{b}, \tau^+\tau^-$. At the LHC, the production of h_{SM} or the CP-even Higgs bosons in the UMSSM is dominated by gluon fusion. We shall focus on gluon fusion in Eq. (17). The production rates of WW^* and ZZ^* reported by CMS and ATLAS are close to the SM predictions:

$$\begin{aligned} 0.2 < R_{WW^*} < 1.1, \quad 0.4 < R_{ZZ^*} < 1.2 & \quad \text{CMS} \\ 0.8 < R_{WW^*} < 1.7, \quad 0.6 < R_{ZZ^*} < 1.8 & \quad \text{ATLAS} \end{aligned}$$

On the other hand, the diphoton production rates reported by CMS [1] and ATLAS [2] are

$$\begin{aligned} 1.1 < R_{\gamma\gamma} < 2.0, \\ 1.3 < R_{\gamma\gamma} < 2.2, \end{aligned}$$

respectively. We require in our scan

$$\begin{aligned} 0.5 < R_{WW^*}, R_{ZZ^*} < 1.5, \\ 1.0 < R_{\gamma\gamma}. \end{aligned} \tag{18}$$

Current limits on the pseudoscalar Higgs boson (A) come from the LEP searches in the associated production with a scalar Higgs boson (H) of $e^+e^- \rightarrow Z^* \rightarrow AH$. In those MSSM-extended models, such as NMSSM, where multiple scalar and pseudoscalar Higgs bosons exist, the constraint could be severe. However, there is only one pseudoscalar Higgs boson in the UMSSM and in our choice of parameters it is often heavier than a few hundred GeV. Thus, it is not constrained by the current limits. Similarly, the charged Higgs boson is also heavy and not constrained by current searches.

B. Numerical results

We start with $h_s = 0.4$ and show relative production rates, as defined by Eq. (17), in Fig. 1. We show $R_{\gamma\gamma}$ versus $\tan\beta$ in part (a), R_{WW^*} versus $R_{\gamma\gamma}$ in part (b), $R_{\gamma\gamma}$ versus m_{h_2} in part (c), and O_{13}^2 versus m_{h_2} in part (d). The majority of the points have $R_{\gamma\gamma}$ between 1.3 and 1.6 while R_{WW^*} (similarly R_{ZZ^*}) is between 1.0 and 1.4 with $\tan\beta$ between 3 and 9. The correlations between $R_{\gamma\gamma}$ and m_{h_2} , and between O_{13}^2 and m_{h_2} show that the enhancement of $R_{\gamma\gamma}$ of h_1 is a result of mixing between the doublet and singlet components. When m_{h_2} gets closer to m_{h_1} , the mixing between h_1 and h_2 gets stronger, and therefore the singlet

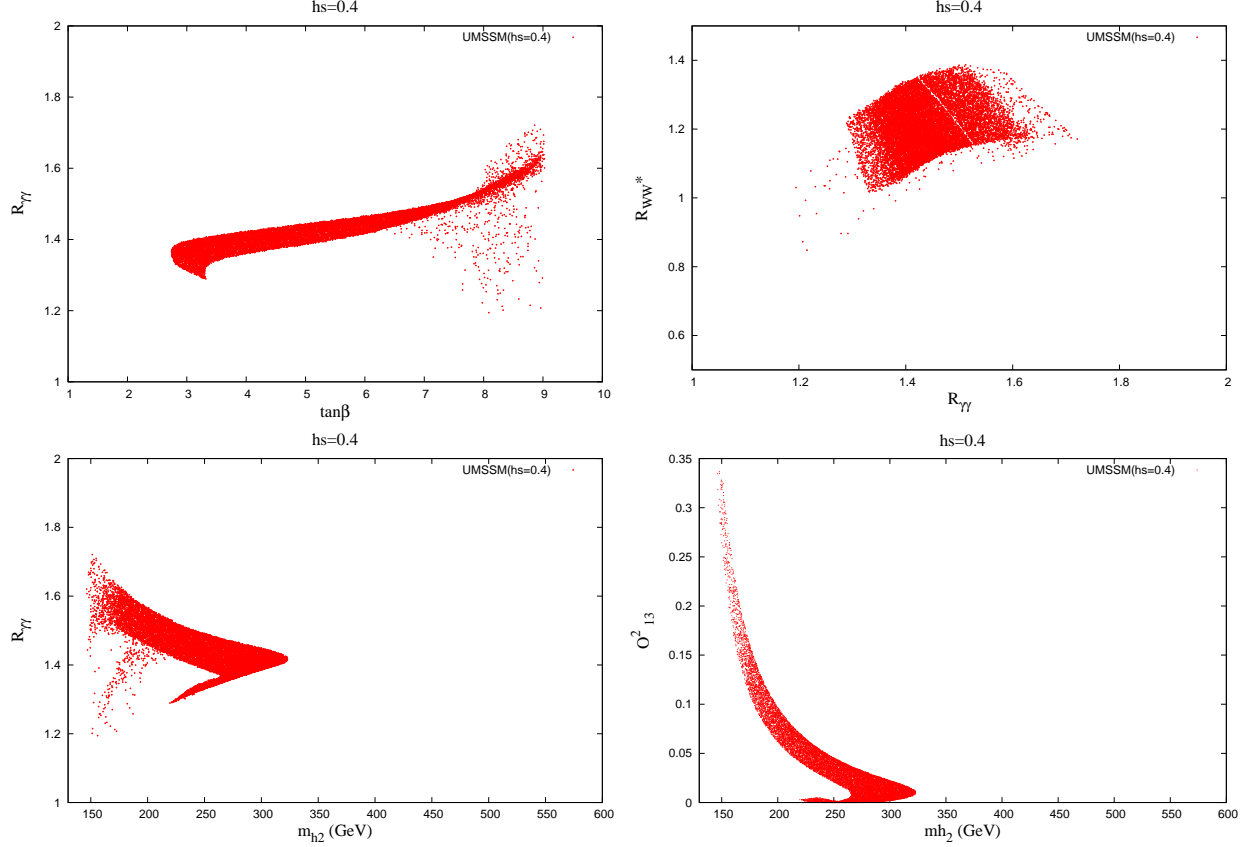


FIG. 1. Case for $h_s = 0.4$. Parameter space points satisfy $124 \text{ GeV} < m_{h_{\text{SM-like}}} < 127 \text{ GeV}$, the chargino mass, and the invisible Z width constraints. Also, the relative production rates satisfy $0.5 < R_{WW^*, ZZ^*} < 1.5$ and $1 < R_{\gamma\gamma}$.

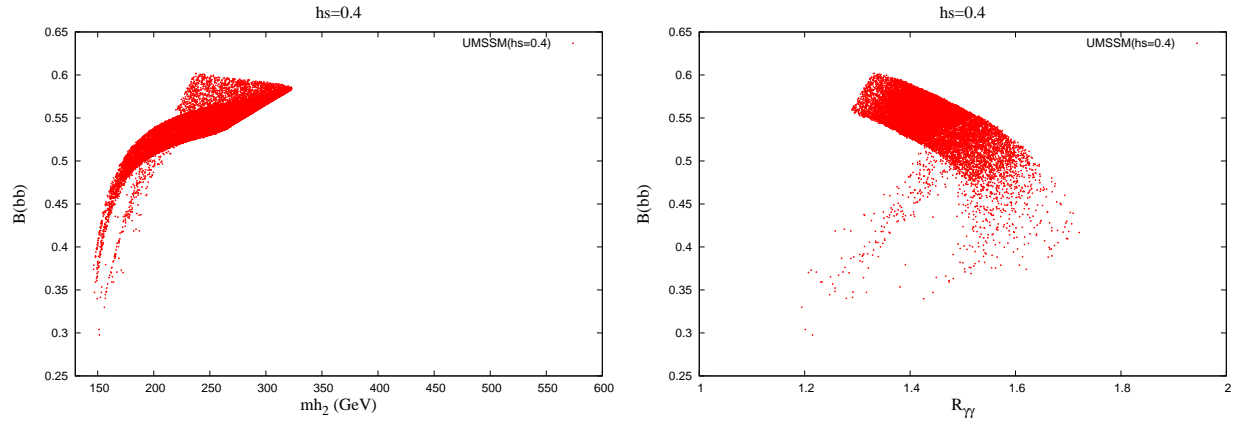


FIG. 2. Case for $h_s = 0.4$. Same as Fig. 1, but showing $B(h_1 \rightarrow b\bar{b})$ versus (a) m_{h_2} and (b) $R_{\gamma\gamma}$.

component O_{13}^2 for h_1 becomes larger and so does $R_{\gamma\gamma}$. The $R_{\gamma\gamma}$ is enhanced mainly due to a reduced total width, which is dominated by the $b\bar{b}$ width. In order to fully understand the enhancement of diphotons, we show the branching ratio $B(h_1 \rightarrow b\bar{b})$ versus (a) m_{h_2} and

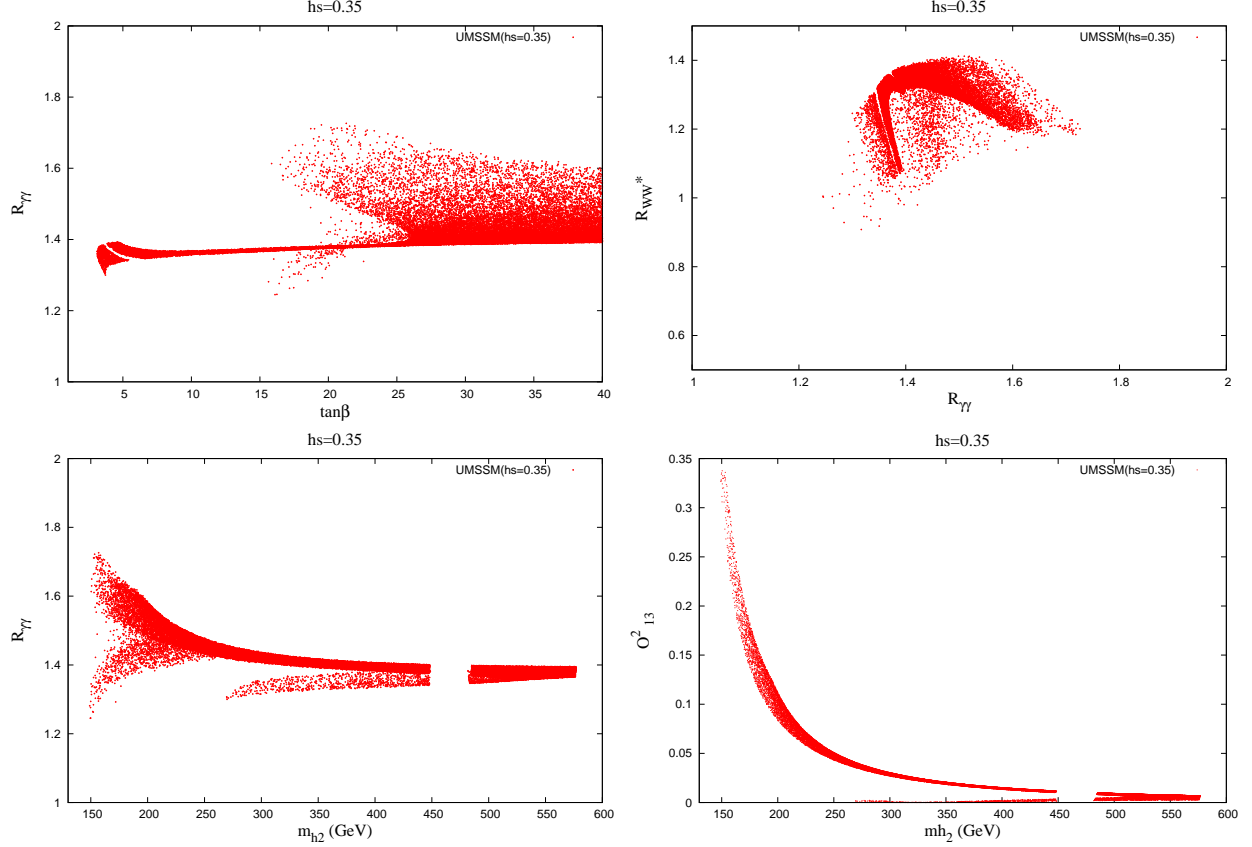


FIG. 3. Same as Fig. 1. Case for $h_s = 0.35$.

(b) $R_{\gamma\gamma}$ in Fig. 2. In Fig. 2 (a) we can see that the branching ratio into $b\bar{b}$ decreases as m_{h_2} approaches m_{h_1} , where the mixing is the strongest. Also, in Fig. 2(b) $R_{\gamma\gamma}$ increases as $B(h_1 \rightarrow b\bar{b})$ decreases. It is now clear that the enhancement in diphotons is due to a reduced $b\bar{b}$ branching ratio, which in turn is because of the stronger mixing with the singlet.

We repeat the cases of $h_s = 0.35$ and $h_s = 0.45$ in Figs. 3 and 4, respectively. It is easy to see that the number of points for $h_s = 0.35$ and $h_s = 0.45$ are reduced substantially as compared with $h_s = 0.4$. The range of $\tan\beta$ for $h_s = 0.35$ stretches between 3 to 40, while for $h_s = 0.45$ it shrinks drastically to between 2.5 and 6. The correlations between R_{WW^*} and $R_{\gamma\gamma}$, between $R_{\gamma\gamma}$ and m_{h_2} , and between O_{13}^2 and m_{h_2} are similar to the case of $h_s = 0.4$. Note that there is a gap in m_{h_2} between 450 – 475 GeV in the case of $h_s = 0.35$, which is mainly due to the combined constraints of $R_{\gamma\gamma}$ and R_{WW^*} . We have checked that there are many fewer points satisfying all the constraints below $h_s = 0.3$ and above $h_s = 0.5$.

An interesting prediction is the relative production rate of $R_{Z\gamma}$, which can probe various Higgs-sector extensions [24]. In the SM, $B(h_{\text{SM}} \rightarrow Z\gamma)$ is smaller than $B(h_{\text{SM}} \rightarrow \gamma\gamma)$.

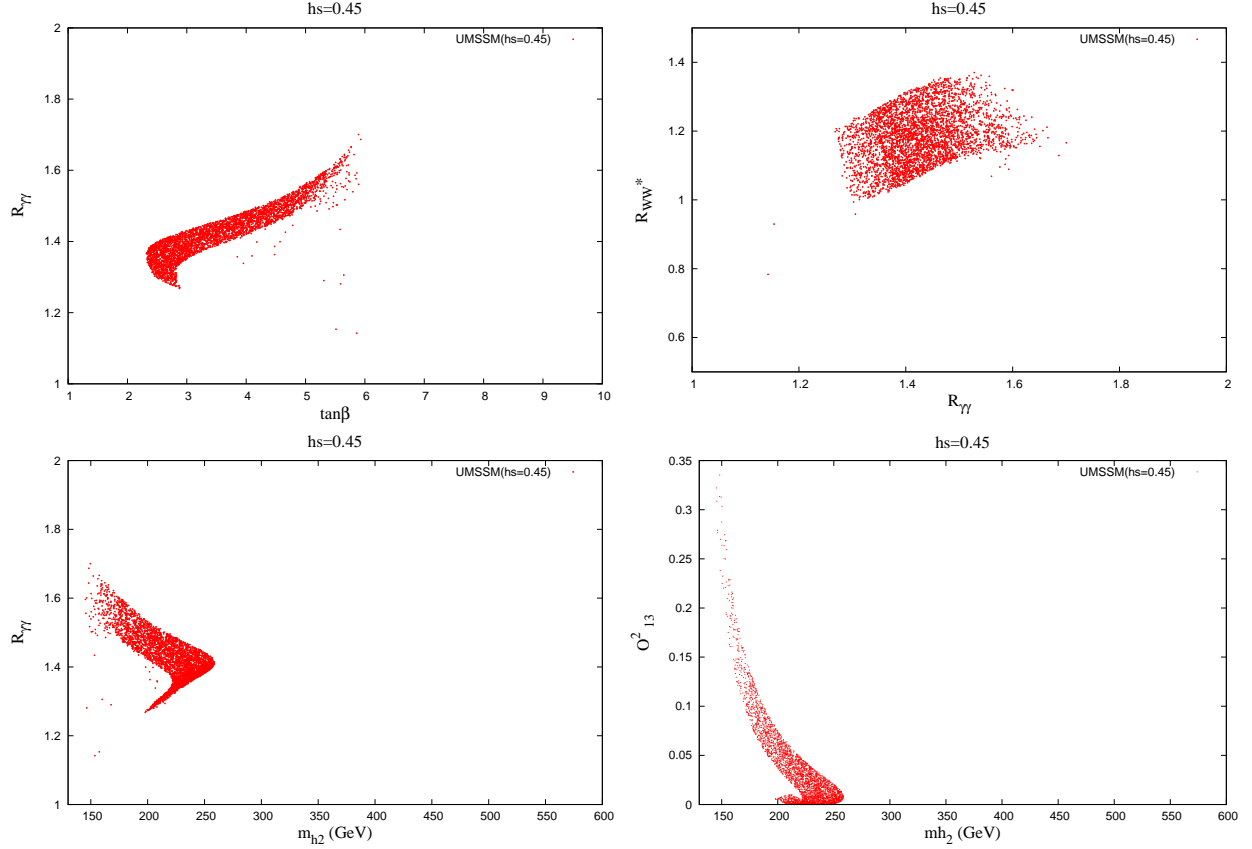


FIG. 4. Same as Fig. 1. Case for $h_s = 0.45$.

We show the correlation between $R_{Z\gamma}$ and $R_{\gamma\gamma}$ for $h_s = 0.35, 0.4, 0.45$ in Fig. 5, in which the points shown already satisfy the constraints listed above. All the points that receive enhancement in the $\gamma\gamma$ channel also receive enhancement in the $Z\gamma$ channel. However, for most of the points $R_{Z\gamma}$ is less than $R_{\gamma\gamma}$, indicated by the points below the green line ($R_{Z\gamma} = R_{\gamma\gamma}$).

It is instructional to list a few selected points in the allowed parameter space, as shown in Table I. The masses $m_{h_{\text{SM-like}}}$ are all around 124 – 126 GeV and m_{h_2} are around 150 – 160 GeV so that the singlet-doublet mixing is strong but not maximal. The $b\bar{b}$ width is reduced by a moderate amount because we have set that the singlet fraction cannot be too large ($O_{13}^2 < 1/3$). Therefore, we can see R_{WW^*} and R_{ZZ^*} are enhanced by about 10 – 15%. The $R_{\gamma\gamma}$ is enhanced by about 60% and $R_{Z\gamma}$ by about 40%. In the future, if experiments can measure $R_{\gamma\gamma}$, R_{WW^*} , and R_{ZZ^*} to better precision, one could tell whether the enhancement in $R_{\gamma\gamma}$ is due to singlet-doublet mixing.

Note that the lightest neutralino $\tilde{\chi}_1^0$ could be lighter than $m_{h_{\text{SM-like}}}/2$. In this case $h_1 \rightarrow$

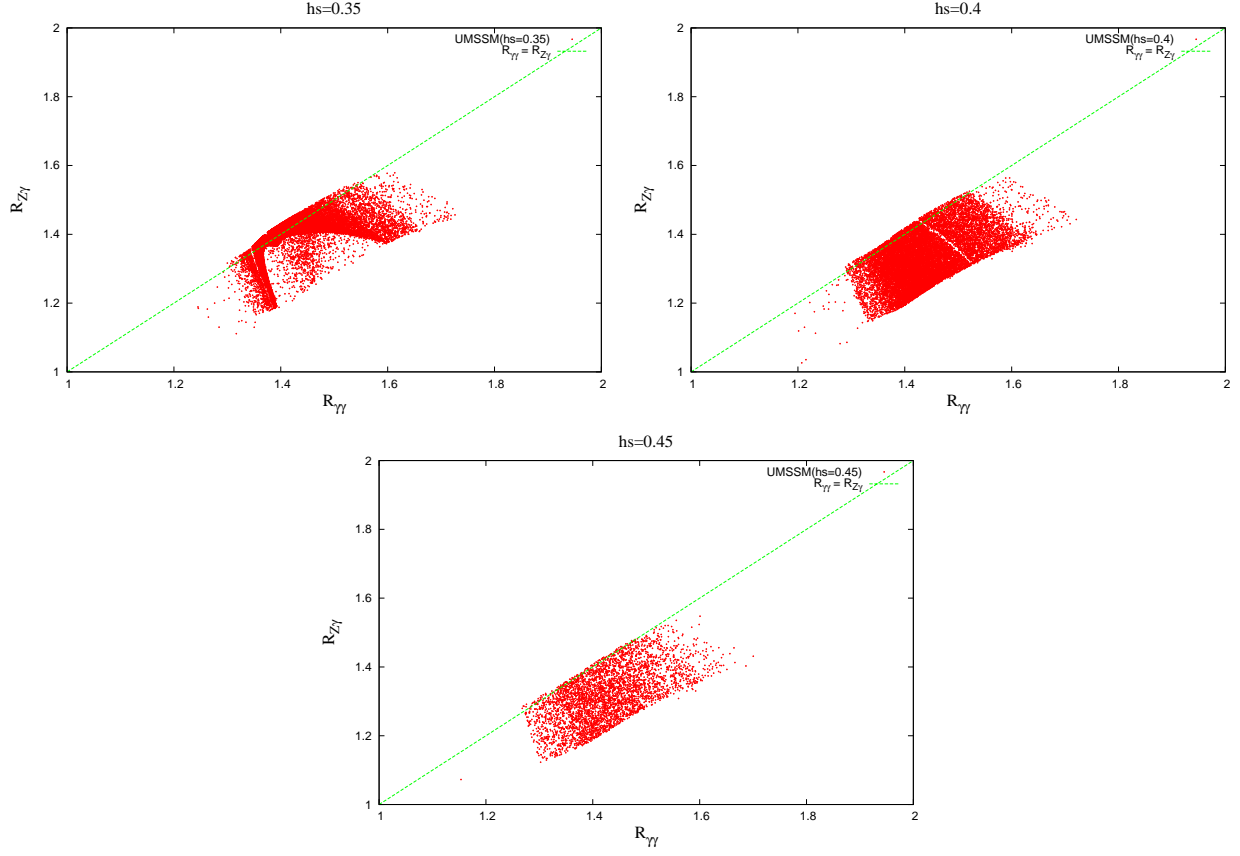


FIG. 5. Correlation between $R_{\gamma\gamma}$ and $R_{Z\gamma}$ for $h_s = 0.35, 0.4, 0.45$.

$\tilde{\chi}_1^0 \tilde{\chi}_1^0$ is possible, but the branching ratio $B(h_1 \rightarrow \tilde{\chi}_1^0 \tilde{\chi}_1^0)$ is very small, because we have set the production rates $R_{\gamma\gamma}$, R_{WW^*} , and R_{ZZ^*} larger than certain values. In Fig. 6, we show the branching ratio of the $B(h_1 \rightarrow \tilde{\chi}_1^0 \tilde{\chi}_1^0)$ (invisible) versus m_{h_2} and O_{13}^2 . These are the parameter-space points satisfying all the constraints of chargino mass, invisible Z width, Higgs boson mass, and the Higgs production rates. We can see that the majority of points are at $B(\text{invisible}) = 0$, because mostly $h_1 \rightarrow \tilde{\chi}_1^0 \tilde{\chi}_1^0$ is not kinematically open yet; while the other points have $B(\text{invisible}) \lesssim 0.25$. This is in accord with a recent model-independent study on the Higgs boson couplings that the nonstandard Higgs decay branching ratio is constrained to be less than about 0.25 [25].

IV. DISCUSSION AND CONCLUSIONS

There are two ways to enhance the diphoton production rate, either by increasing the absolute width into $\gamma\gamma$ or by reducing the total width of the Higgs boson (which is dominated

TABLE I. Selected points (labeled 1, 2, and 3) in the allowed parameter space for $h_s = 0.35, 0.4, 0.45$. The masses are given in GeV. The $h_{\text{SM-like}} = h_1$ in our scan.

	$h_s = 0.35$			$h_s = 0.4$			$h_s = 0.45$		
	No. 1	No. 2	No. 3	No. 1	No. 2	No. 3	No. 1	No. 2	No. 3
$m_{h_{\text{SM-like}}}$	124.42	124.02	126.04	124.02	124.01	125.45	124.13	125.51	124.35
m_{h_2}	154.49	157.15	162.80	159.23	158.27	149.30	159.59	158.88	149.48
$m_{\tilde{\chi}_0}$	54.32	27.77	64.61	28.75	25.33	64.71	27.84	87.70	67.11
$ O_{13} ^2$	0.316	0.296	0.210	0.248	0.256	0.319	0.215	0.188	0.313
$\tan \beta$	19.91	21.55	19.53	9.01	9.01	8.46	5.74	5.53	5.89
$B(h \rightarrow \gamma\gamma) \times 10^3$	4.23	4.31	3.73	3.83	3.90	4.43	3.75	3.62	4.41
$B(h \rightarrow b\bar{b})$	0.387	0.425	0.441	0.444	0.443	0.400	0.480	0.473	0.428
$B(h \rightarrow \tilde{\chi}_1^0 \tilde{\chi}_1^0)$	0.054	0.007	0.0	0.039	0.033	0.0	0.009	0.0	0.0
$R_{\gamma\gamma}$	1.63	1.72	1.61	1.63	1.64	1.66	1.65	1.61	1.70
R_{ZZ^*}	1.15	1.18	1.38	1.13	1.13	1.27	1.16	1.29	1.17
R_{WW^*}	1.15	1.18	1.34	1.13	1.14	1.25	1.16	1.26	1.17
$R_{Z\gamma}$	1.40	1.44	1.53	1.36	1.37	1.50	1.39	1.47	1.43

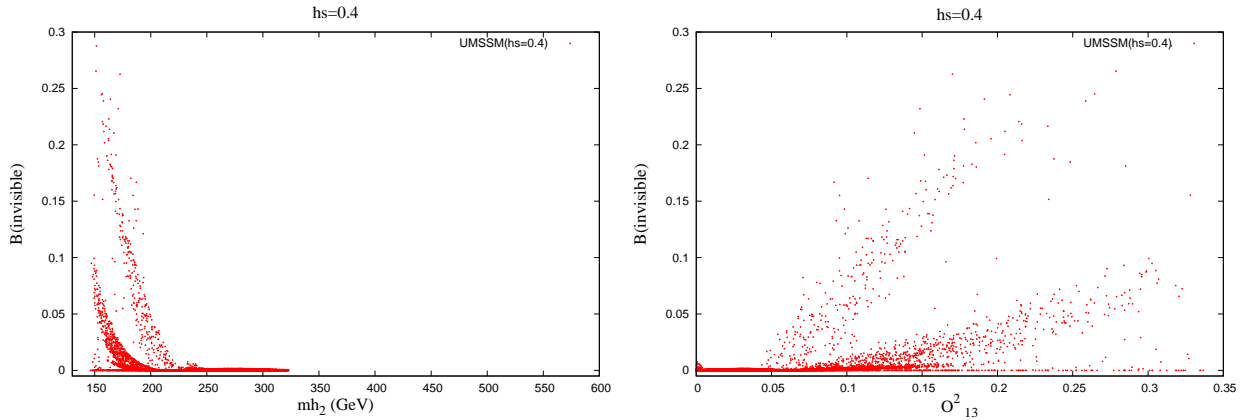


FIG. 6. Case for $h_s = 0.4$. Same as Fig. 1. Shown is the invisible branching ratio $B(h_1 \rightarrow \tilde{\chi}_1^0 \tilde{\chi}_1^0)$ versus (a) m_{h_2} and (b) O_{13}^2 .

by the $b\bar{b}$ width at 125 GeV). The former is possible if an extra light charged particle is running in the triangular loop, e.g., a light stau [4], in the MSSM. The latter effect is possible if the SM-like Higgs boson has a large mixing with another singlet-like Higgs boson,

e.g., in the NMSSM [8], such that the $b\bar{b}$ width is reduced by the mixing and therefore the $\gamma\gamma$ branching ratio is enhanced.

For the choice of UMSSM parameters all the extra charged particles like the stau, top squark, sbottom and the charged Higgs boson are relatively heavy. We have searched in the parameter space of UMSSM under the constraints of current Higgs boson data, chargino-mass bound, and Z invisible width. We found that (1) the enhancement of the diphoton production rate is mainly due to the mixing between the Higgs doublets and singlet, and (2) the lightest CP-even Higgs boson is SM-like while the second lightest is more singletlike. This is in contrast to the case of NMSSM, in which the lightest is singletlike and the second lightest is SM-like.

Before closing, we offer a few more comments as follows.

1. The relative production rate $R_{Z\gamma}$ mostly goes in the same direction as $R_{\gamma\gamma}$, though the amount of enhancement in $R_{Z\gamma}$ is less than $R_{\gamma\gamma}$. The probing of the $Z\gamma$ mode of the observed Higgs boson is an interesting test for the Higgs boson from the SM or from its extensions. In the present luminosity, it is rather difficult to probe the $Z\gamma$ because it suffers an additional suppression from the leptonic branching ratio of the Z boson.
2. Almost all of the points have R_{WW^*} between 1.0 and 1.4. This is easy to understand because $R_{\gamma\gamma}$ is enhanced by a reduced total width. Therefore, the WW^* and ZZ^* branching ratios also increase.
3. The mass of the second lightest CP-even Higgs boson cannot be too large, as shown in bottom panels of Figs. 1, 3, 4. Again, this is easy to understand because in order to achieve a large doublet-singlet mixing between h_1 and h_2 their mass difference cannot be too large. We found that $m_{h_2} < 580, 320, 260$ GeV for $h_s = 0.35, 0.4, 0.45$ respectively. The detection of h_2 is rather difficult because of its singlet nature. The production cross section would be reduced significantly by the mixing.
4. There are six physical neutralinos in the mass spectrum in UMSSM. The lightest one can be the dark matter candidate. If kinematics is allowed, it may lead to invisible modes for the decays of Higgs bosons, Z' or even Z . Dark matter physics is therefore very rich in this model. We only touch upon this lightly in this work and would like to return to this issue in future publications.

Appendix A: Loop Functions

The partial decay width for $h_j \rightarrow \gamma\gamma$ is given by Eq.(6). The loop functions are given by

$$F_f = -2x_f [1 + (1 - x_f) f(x_f)] R_f \quad (f = \tau, t, b) \quad (\text{A1})$$

$$F_W = [2 + 3x_W + 3x_W (2 - x_W) f(x_W)] R_W \quad (\text{A2})$$

$$F_{h^\pm} = x_{h^\pm} [1 - x_{h^\pm} f(x_{h^\pm})] R_{h^\pm} \frac{m_W^2}{m_{h^\pm}^2} \quad (\text{A3})$$

for non-SUSY particles and

$$F_{\tilde{f}} = \sum_{i=1,2} x_{\tilde{f}_i} [1 - x_{\tilde{f}_i} f(x_{\tilde{f}_i})] R_{h_j \tilde{f}_i \tilde{f}_i} \frac{m_Z^2}{m_{\tilde{f}_i}^2} \quad (\tilde{f} = \tilde{\tau}, \tilde{t}, \tilde{b}) \quad (\text{A4})$$

$$F_{\tilde{\chi}^\pm} = \sum_{i=1,2} -2x_{\tilde{\chi}_i^\pm} \left[1 + \left(1 - x_{\tilde{\chi}_i^\pm} \right) f(x_{\tilde{\chi}_i^\pm}) \right] R_{\tilde{\chi}_i^\pm} \frac{m_W}{m_{\tilde{\chi}_i^\pm}} \quad (\text{A5})$$

for sparticles with $x_X = 4m_X^2/m_{h_j}^2$ ($X = \tau, t, b, W, h^\pm, \tilde{\tau}, \tilde{t}, \tilde{b}, \tilde{\chi}_i^\pm$).

$$f(x) = \begin{cases} \left[\sin^{-1} \sqrt{\frac{1}{x}} \right]^2 & \text{for } x \geq 1 \\ -\frac{1}{4} \left[\ln \left(\frac{1+\sqrt{1-x}}{1-\sqrt{1-x}} \right) - i\pi \right]^2 & \text{for } x < 1 \end{cases} \quad (\text{A6})$$

The couplings entering into the loop functions for the non-SUSY particles are

$$R_\tau = \frac{O_{j1}}{\cos \beta}, \quad R_t = \frac{O_{j2}}{\sin \beta}, \quad R_b = R_\tau \quad (\text{A7})$$

$$R_W = O_{j2} \sin \beta + O_{j1} \cos \beta \quad (\text{A8})$$

$$\begin{aligned} R_{h^\pm} = & \frac{3 - 2 \sin^2 \theta_W}{2 \cos^2 \theta_W} \sin \beta \cos \beta (O_{j2} \cos \beta + O_{j1} \sin \beta) \\ & + \frac{1 - 2 \sin^2 \theta_W}{2 \cos^2 \theta_W} (O_{j2} \sin^3 \beta + O_{j1} \cos^3 \beta) \\ & + \frac{2g_2^2}{g^2} Q'_{H_u}{}^2 O_{j2} \sin \beta \cos^2 \beta + \frac{2g_2^2}{g^2} Q'_{H_d}{}^2 O_{j1} \sin^2 \beta \cos \beta \\ & + \frac{2g_2^2}{g^2} Q'_{H_u} Q'_{H_d} (O_{j2} \sin^3 \beta + O_{j1} \cos^3 \beta) \\ & - \frac{2h_s^2}{g^2} \sin \beta \cos \beta (O_{j2} \cos \beta + O_{j1} \sin \beta) \\ & + \left(\frac{h_s^2 v_s}{gm_W} + \frac{g_2^2}{gm_W} Q'_{H_u} Q'_S v_s \cos^2 \beta + \frac{g_2^2}{gm_W} Q'_{H_d} Q'_S v_s \sin^2 \beta \right. \\ & \left. + \frac{\sqrt{2} h_s A_s}{gm_W} \sin \beta \cos \beta \right) O_{j3} \end{aligned} \quad (\text{A9})$$

For the sfermions, we have the couplings

$$R_{h_j \tilde{f}_1 \tilde{f}_1} = R_{\tilde{f}}^L \cos^2 \theta_{\tilde{f}} + R_{\tilde{f}}^R \sin^2 \theta_{\tilde{f}} + 2R_{\tilde{f}}^{RL} \sin \theta_{\tilde{f}} \cos \theta_{\tilde{f}} \quad (\text{A10})$$

$$R_{h_j \tilde{f}_2 \tilde{f}_2} = R_{\tilde{f}}^L \sin^2 \theta_{\tilde{f}} + R_{\tilde{f}}^R \cos^2 \theta_{\tilde{f}} - 2R_{\tilde{f}}^{RL} \sin \theta_{\tilde{f}} \cos \theta_{\tilde{f}} \quad (\text{A11})$$

where $\theta_{\tilde{f}}$ is the mixing angle between \tilde{f}_L and \tilde{f}_R to obtain the physical mass eigenstates \tilde{f}_1 and \tilde{f}_2 . For the $Z\gamma$ case, we also need the off-diagonal term

$$R_{h_j \tilde{f}_1 \tilde{f}_2} = (R_{\tilde{f}}^R - R_{\tilde{f}}^L) \sin \theta_{\tilde{f}} \cos \theta_{\tilde{f}} + R_{\tilde{f}}^{RL} (\cos^2 \theta_{\tilde{f}} - \sin^2 \theta_{\tilde{f}}) . \quad (\text{A12})$$

The expressions of $R_{\tilde{t},\tilde{b}}^{L,R,RL}$ are given by

$$\begin{aligned} R_{\tilde{t},\tilde{b}}^L = & \frac{vm_W}{gm_Z^2} \left[\left(\frac{g^2}{2 \cos^2 \theta_W} (\sin^2 \theta_W Q^{t,b} - T_3^{t,b}) + g_2^2 Q'_{H_u} Q'_{Q_3} \right) O_{j2} \sin \beta + \frac{2m_{t,b}^2}{v^2} R_{t,b} \right. \\ & + \left(-\frac{g^2}{2 \cos^2 \theta_W} (\sin^2 \theta_W Q^{t,b} - T_3^{t,b}) + g_2^2 Q'_{H_d} Q'_{Q_3} \right) O_{j1} \cos \beta \\ & \left. + g_2^2 \frac{v_s}{v} Q'_S Q'_{Q_3} O_{j3} \right] \end{aligned} \quad (\text{A13})$$

$$\begin{aligned} R_{\tilde{t},\tilde{b}}^R = & \frac{vm_W}{gm_Z^2} \left[\left(-\frac{g^2 \sin^2 \theta_W}{2 \cos^2 \theta_W} Q^{t,b} + g_2^2 Q'_{H_u} Q'_{U_3^c, D_3^c} \right) O_{j2} \sin \beta + \frac{2m_{t,b}^2}{v^2} R_{t,b} \right. \\ & \left. + \left(\frac{g^2 \sin^2 \theta_W}{2 \cos^2 \theta_W} Q^{t,b} + g_2^2 Q'_{H_d} Q'_{U_3^c, D_3^c} \right) O_{j1} \cos \beta + g_2^2 \frac{v_s}{v} Q'_S Q'_{U_3^c, D_3^c} O_{j3} \right] \end{aligned} \quad (\text{A14})$$

$$R_{\tilde{t},\tilde{b}}^{RL} = \frac{vm_{t,b}}{2m_W^2} \left(\frac{g}{2m_W} A_{t,b} R_{t,b} - h_s \left[\frac{gv_s}{2\sqrt{2}m_W} R'_{t,b} - \frac{1}{\sqrt{2}} R''_{t,b} \right] \right) \quad (\text{A15})$$

where we have defined

$$R'_\tau = \frac{O_{j2}}{\cos \beta} , \quad R'_t = \frac{O_{j1}}{\sin \beta} , \quad R'_b = R'_\tau \quad (\text{A16})$$

$$R''_\tau = O_{j3} \tan \beta , \quad R''_t = O_{j3} \cot \beta , \quad R''_b = R''_\tau \quad (\text{A17})$$

The $R_{\tilde{\tau}}^{L,R,RL}$ can be obtained from the $R_{\tilde{b}}^{L,R,RL}$ by appropriate substitutions.

For the chargino loop, we have

$$R_{\tilde{\chi}_i^\pm} = 2 \left[\frac{1}{\sqrt{2}} V_{i1} U_{i2} O_{j1} + \frac{1}{\sqrt{2}} V_{i2} U_{i1} O_{j2} + \frac{h_s}{\sqrt{2}g} V_{i2} U_{i2} O_{j3} \right] , \quad (\text{A18})$$

where U and V are the two unitary matrices that diagonalize the chargino mass matrix.

The partial decay width for $h_j \rightarrow Z\gamma$ is given by Eq.(8). The loop functions for the non-SUSY particles are given by

$$G_f = N_C^f \cdot R_f \cdot \frac{-2Q^f [T_3^f - 2Q^f \sin^2 \theta_W]}{\sin \theta_W \cos \theta_W} [I_1(\tau_f, \lambda_f) - I_2(\tau_f, \lambda_f)] \quad (f = \tau, t, b) \quad (\text{A19})$$

$$G_W = -R_W \cot \theta_W \left(4 (3 - \tan^2 \theta_W) I_2(\tau_W, \lambda_W) + \left[\left(1 + \frac{2}{\tau_W} \right) \tan^2 \theta_W - \left(5 + \frac{2}{\tau_W} \right) \right] I_1(\tau_W, \lambda_W) \right) \quad (\text{A20})$$

$$G_{h^\pm} = R_{h^\pm} \frac{1 - 2 \sin^2 \theta_W}{\sin \theta_W \cos \theta_W} I_1(\tau_{h^\pm}, \lambda_{h^\pm}) \frac{m_W^2}{m_{h^\pm}^2} \quad (\text{A21})$$

Here, we define

$$\tau_X = \frac{4m_X^2}{m_{h_j}^2}, \quad \lambda_X = \frac{4m_X^2}{m_Z^2} \quad (X = \tau, t, b, W, h^\pm). \quad (\text{A22})$$

The definitions of $I_1(\tau, \lambda)$ and $I_2(\tau, \lambda)$ are the same as given in [26].

$$I_1(\tau, \lambda) = \frac{\tau \lambda}{2(\tau - \lambda)} + \frac{\tau^2 \lambda^2}{2(\tau - \lambda)^2} [f(\tau) - f(\lambda)] + \frac{\tau^2 \lambda}{(\tau - \lambda)^2} [g(\tau) - g(\lambda)] \quad (\text{A23})$$

$$I_2(\tau, \lambda) = -\frac{\tau \lambda}{2(\tau - \lambda)} [f(\tau) - f(\lambda)] \quad (\text{A24})$$

where $f(x)$ is given in Eq.(A6) and $g(x)$ is defined as

$$g(x) = \begin{cases} \sqrt{x-1} \left[\sin^{-1} \sqrt{\frac{1}{x}} \right] & \text{for } x \geq 1 \\ \frac{1}{2} \sqrt{1-x} \left[\ln \left(\frac{1+\sqrt{1-x}}{1-\sqrt{1-x}} \right) - i\pi \right] & \text{for } x < 1 \end{cases} \quad (\text{A25})$$

For the sparticles, we have

$$G_{\tilde{f}} = 8 \cdot N_C^f \cdot Q^f \cdot m_Z^2 \sum_{k,l=1,2} R_{h_j \tilde{f}_l \tilde{f}_k} R_{Z \tilde{f}_k \tilde{f}_l} C_2(m_{\tilde{f}_l}, m_{\tilde{f}_k}, m_{\tilde{f}_k}) \quad (\text{A26})$$

$$G_{\tilde{\chi}^\pm} = \sum_{k,l=1,2} \frac{m_Z m_{\tilde{\chi}_l^+}}{\sin \theta_W} f(m_{\tilde{\chi}_l^+}, m_{\tilde{\chi}_k^+}, m_{\tilde{\chi}_k^+}) \sum_{m,n=L,R} R_{Z \tilde{\chi}_l^+ \tilde{\chi}_k^-}^m R_{h_j \tilde{\chi}_k^+ \tilde{\chi}_l^-}^n \quad (\text{A27})$$

The definitions of $C_2(m_1, m_2, m_2)$ and $f(m_1, m_2, m_2)$ can be found in [27]. The couplings for the sfermions are

$$R_{Z \tilde{f}_1 \tilde{f}_1} = \frac{1}{\sin \theta_W \cos \theta_W} \left[(T_3^f - Q^f \sin^2 \theta_W) \cos^2 \theta_{\tilde{f}} - Q^f \sin^2 \theta_W \sin^2 \theta_{\tilde{f}} \right] \quad (\text{A28})$$

$$R_{Z \tilde{f}_2 \tilde{f}_2} = \frac{1}{\sin \theta_W \cos \theta_W} \left[-Q^f \sin^2 \theta_W \cos^2 \theta_{\tilde{f}} + (T_3^f - Q^f \sin^2 \theta_W) \sin^2 \theta_{\tilde{f}} \right] \quad (\text{A29})$$

$$R_{Z \tilde{f}_1 \tilde{f}_2} = \frac{-T_3^f}{\sin \theta_W \cos \theta_W} \sin \theta_{\tilde{f}} \cos \theta_{\tilde{f}} \quad (\text{A30})$$

For the charginos, the couplings are

$$R_{Z\tilde{\chi}_i^+\tilde{\chi}_k^-}^L = - \left(V_{l1}V_{k1} + \frac{1}{2}V_{l2}V_{k2} - \delta_{lk}\sin^2\theta_W \right) \quad (\text{A31})$$

$$R_{Z\tilde{\chi}_i^+\tilde{\chi}_k^-}^R = - \left(U_{l1}U_{k1} + \frac{1}{2}U_{l2}U_{k2} - \delta_{lk}\sin^2\theta_W \right) \quad (\text{A32})$$

$$R_{h_j\tilde{\chi}_i^+\tilde{\chi}_l^-}^L = \frac{1}{\sqrt{2}} \left[V_{l1}U_{i2}O_{j1} + V_{l2}U_{i1}O_{j2} + \frac{h_s}{g}V_{l2}U_{i2}O_{j3} \right] \quad (\text{A33})$$

$$R_{h_j\tilde{\chi}_i^+\tilde{\chi}_l^-}^R = \frac{1}{\sqrt{2}} \left[V_{i1}U_{l2}O_{j1} + V_{i2}U_{l1}O_{j2} + \frac{h_s}{g}V_{i2}U_{l2}O_{j3} \right] \quad (\text{A34})$$

The partial decay width for $h_j \rightarrow gg$ is given by Eq.(7). The loop functions F_f and $F_{\tilde{f}}$ for the colored particles are the same as in the case of $h_j \rightarrow \gamma\gamma$ given by Eqs.(A1) and (A4) respectively.

ACKNOWLEDGMENTS

This work was supported in parts by the National Science Council of Taiwan under Grants No. 99-2112-M-007-005-MY3 and No. 101-2112-M-001-005-MY3, and the WCU program through the KOSEF funded by the MEST (R31-2008-000-10057-0). TCY is grateful to the National Center for Theoretical Sciences of Taiwan for its warm hospitality.

-
- [1] S. Chatrchyan *et al.* [CMS Collaboration], Phys. Lett. B **716**, 30 (2012) [arXiv:1207.7235 [hep-ex]].
 - [2] G. Aad *et al.* [ATLAS Collaboration], Phys. Lett. B **716**, 1 (2012) [arXiv:1207.7214 [hep-ex]].
 - [3] See e.g., H. Baer, V. Barger and A. Mustafayev, Phys. Rev. D **85**, 075010 (2012) [arXiv:1112.3017 [hep-ph]]; S. Heinemeyer, O. Stal and G. Weiglein, Phys. Lett. B **710**, 201 (2012) [arXiv:1112.3026 [hep-ph]]; A. Arbey, M. Battaglia, A. Djouadi, F. Mahmoudi and J. Quevillon, Phys. Lett. B **708**, 162 (2012) [arXiv:1112.3028 [hep-ph]]; P. Draper, P. Meade, M. Reece and D. Shih, Phys. Rev. D **85**, 095007 (2012) [arXiv:1112.3068 [hep-ph]]; S. Akula, B. Altunkaynak, D. Feldman, P. Nath and G. Peim, Phys. Rev. D **85**, 075001 (2012) [arXiv:1112.3645 [hep-ph]]; M. Kadastik, K. Kannike, A. Racioppi and M. Raidal, JHEP **1205**, 061 (2012) [arXiv:1112.3647 [hep-ph]]; J. Cao, Z. Heng, D. Li and J. M. Yang,

- Phys. Lett. B **710**, 665 (2012) [arXiv:1112.4391 [hep-ph]]; J. L. Feng and D. Sanford, Phys. Rev. D **86**, 055015 (2012) [arXiv:1205.2372 [hep-ph]].
- [4] M. Carena, S. Gori, N. R. Shah, C. E. M. Wagner and L. -T. Wang, JHEP **1207**, 175 (2012) [arXiv:1205.5842 [hep-ph]]; M. Carena, S. Gori, N. R. Shah and C. E. M. Wagner, JHEP **1203**, 014 (2012) [arXiv:1112.3336 [hep-ph]].
- [5] A. Drozd, B. Grzadkowski, J. F. Gunion and Y. Jiang, arXiv:1211.3580 [hep-ph].
- [6] N. D. Christensen, T. Han and S. Su, Phys. Rev. D **85**, 115018 (2012) [arXiv:1203.3207 [hep-ph]]; K. Hagiwara, J. S. Lee and J. Nakamura, JHEP **1210**, 002 (2012) [arXiv:1207.0802 [hep-ph]].
- [7] V. Barger, M. Ishida and W. -Y. Keung, arXiv:1207.0779 [hep-ph].
- [8] U. Ellwanger, JHEP **1203**, 044 (2012) [arXiv:1112.3548 [hep-ph]]; U. Ellwanger and C. Hugonie, Adv. High Energy Phys. **2012**, 625389 (2012) [arXiv:1203.5048 [hep-ph]].
- [9] J. F. Gunion, Y. Jiang and S. Kraml, Phys. Lett. B **710**, 454 (2012) [arXiv:1201.0982 [hep-ph]]; S. F. King, M. Muhlleitner and R. Nevzorov, Nucl. Phys. B **860**, 207 (2012) [arXiv:1201.2671 [hep-ph]]; D. A. Vasquez, G. Belanger, C. Boehm, J. Da Silva, P. Richardson and C. Wymant, Phys. Rev. D **86**, 035023 (2012) [arXiv:1203.3446 [hep-ph]]; J. -J. Cao, Z. -X. Heng, J. M. Yang, Y. -M. Zhang and J. -Y. Zhu, JHEP **1203**, 086 (2012) [arXiv:1202.5821 [hep-ph]]; K. Kowalska, S. Munir, L. Roszkowski, E. M. Sessolo, S. Trojanowski and Y. -L. S. Tsai, arXiv:1211.1693 [hep-ph].
- [10] K. Schmidt-Hoberg and F. Staub, JHEP **1210**, 195 (2012) [arXiv:1208.1683 [hep-ph]].
- [11] For a review, see P. Langacker, Rev. Mod. Phys. **81**, 1199-1228 (2009) [arXiv:0801.1345 [hep-ph]].
- [12] C. -F. Chang, K. Cheung and T. -C. Yuan, JHEP **1109** 058 (2011) [arXiv:1107.1133 [hep-ph]].
- [13] J. Kang and P. Langacker, Phys. Rev. **D71**, 035014 (2005) [hep-ph/0412190]; M. Baumgart, T. Hartman, C. Kilic and L. -T. Wang, JHEP **0711**, 084 (2007). [hep-ph/0608172].
- [14] C. -F. Chang, K. Cheung, Y. -C. Lin and T. -C. Yuan, JHEP **1206**, 128 (2012) [arXiv:1202.0054 [hep-ph]].
- [15] H. An, T. Liu and L. -T. Wang, arXiv:1207.2473 [hep-ph].
- [16] A. Alves, A. G. Dias, E. R. Barreto, C. A. de S. Pires, F. S. Queiroz and P. S. R. da Silva, arXiv:1207.3699 [hep-ph].

- [17] V. Barger, P. Langacker and H. -S. Lee, Phys. Lett. **B630**, 85-99 (2005) [hep-ph/0508027];
V. Barger, P. Langacker and G. Shaughnessy, Phys. Lett. **B644**, 361-369 (2007) [hep-ph/0609068].
- [18] V. Barger, P. Langacker and G. Shaughnessy, Phys. Rev. **D75**, 055013 (2007) [hep-ph/0611239]; V. Barger, P. Langacker, H. -S. Lee and G. Shaughnessy, Phys. Rev. **D73**, 115010 (2006) [hep-ph/0603247].
- [19] S. Y. Choi, H. E. Haber, J. Kalinowski and P. M. Zerwas, Nucl. Phys. B **778**, 85 (2007) [hep-ph/0612218].
- [20] S. Chatrchyan *et al.* [CMS Collaboration], Phys. Lett. B **704**, 123 (2011) [arXiv:1107.4771 [hep-ex]].
- [21] T. Aaltonen *et al.* [CDF Collaboration], Phys. Rev. D **79**, 112002 (2009) [arXiv:0812.4036 [hep-ex]].
- [22] K. Cheung and J. Song, Phys. Rev. Lett. **106**, 211803 (2011) [arXiv:1104.1375 [hep-ph]].
- [23] K. Nakamura *et al.* (Particle Data Group), J. Phys. G **37**, No 7A, 075021 (2010).
- [24] C. -W. Chiang, K. Yagyu and K. Yagyu, arXiv:1207.1065 [hep-ph].
- [25] K. Cheung, J. S. Lee and P. -Y. Tseng, arXiv:1302.3794 [hep-ph].
- [26] J. F. Gunion, H. E. Haber, G. L. Kane and S. Dawson, “The Higgs Hunter’s Guide,” published in Front. Phys. **80**, 1 (2000) page 29.
- [27] A. Djouadi, V. Driesen, W. Hollik and A. Kraft, Eur. Phys. J. C **1**, 163 (1998) [hep-ph/9701342].